

# Magneto-transport behaviors in molybdenum silicide amorphous thin films

Zhengyuan Liu, Bingcheng Luo <sup>a)</sup>, Junbiao Hu, Cheng Xing

Department of Applied Physics, Northwestern Polytechnical University, Xi'an, 710072, China

<sup>a)</sup> Electronic mail: [luobingcheng@nwpu.edu.cn](mailto:luobingcheng@nwpu.edu.cn)

## Abstract

Molybdenum silicide amorphous compounds have attracted significant interest for ultrasensitive thermometer applications because of their high uniformity, and tunable superconducting transition temperature. In comparison to the extensively investigated superconducting characteristics, however, the transport mechanism in non-superconducting region is still little-known. In this work, through the temperature-dependent electronic transport and magneto-resistance measurements in non-superconducting region, the Mott variable range hopping conductivity was demonstrated and crossover from positive to negative magneto-resistance was revealed in sputtered molybdenum silicide films.

Keywords: Amorphous films, Molybdenum silicide, Magneto-resistance, Variable range hopping conductivity

## 1. Introduction

Transition metal (TM) based amorphous materials have been studied in recent years due to their unique properties such as high uniformity, lower carrier density and stability of the amorphous structure [1-3]. What's more, the discovery of superconductivity in transition-metal amorphous alloys [4] further trigger general research interest. Among TM-based amorphous materials, molybdenum-based amorphous compounds have attracted a significant research due to their tunable superconducting transition temperature [5], intrinsically low flux pinning and homogeneity [6-9]. These excellent characteristics make them competitive alternatives for superconducting single photon detectors [10-13]. Additionally, molybdenum-based amorphous compounds also exhibit tantalizing research interest in vortex dynamics, enabling them to optimize device performances [14]. So far, considerable efforts have been attributed to the electronic transport and magneto-transport behaviors of the molybdenum-based amorphous compounds around the superconducting state [7, 15-18]. By contrast, the investigation of molybdenum-based amorphous compounds in non-superconducting region is insufficient, but it is important for developing deeper physical insight into transport behaviors and further exploring potential applications [3]. Therefore, we here studied the electronic transport and magneto-transport behaviors of sputtered molybdenum silicide amorphous films in non-superconducting region. Magneto-transport measurement is a powerful method to reveal the underneath transport mechanism in many crystalline and amorphous materials [19]. The extensive report about magneto-resistance (MR) in amorphous compounds dates back to 1970s in the case of Ge, Si, InSb and GeTe [20]. The crossover of positive and negative MR was reported in some materials such as  $\text{Ni}_x\text{Si}_{1-x}$  and  $\text{Mo}_x\text{Ge}_{1-x}$  [21, 22]. In molybdenum-based amorphous compounds, however, the report of analogous MR behavior is still lacking.

## 2. Methods

Molybdenum silicide films (MoSi) with thickness of 30 nm were deposited on silicon ( $>10^5 \Omega \text{ cm}$ ) at room temperature by radio-frequency (RF) magnetron sputtering technique. The base pressure of the chamber is less than  $1 \times 10^{-4}$  Pa. The RF power intensity is  $2 \text{ W cm}^{-1}$ . The sputtering pressure is 20 m Torr in pure argon ambient. Prior to deposition, the target is pre-sputtered for 30 min to eliminate the influence of target surface. A commercial atomic force microscopy (AFM) (MFP-3D, Asylum Research) was used to measure the surface topography. The film chemical compositions were determined by X-ray photoelectron spectroscopy (XPS, ESCALAB 250) with Al  $K\alpha$  radiation. The temperature-dependent and magnetic-field dependent resistances were measured by a physical property measurement system (Cryogenic CFMS-14T) using the four-probe method. The magnetic field was applied perpendicular to the sample.

### 3. Results and Discussion

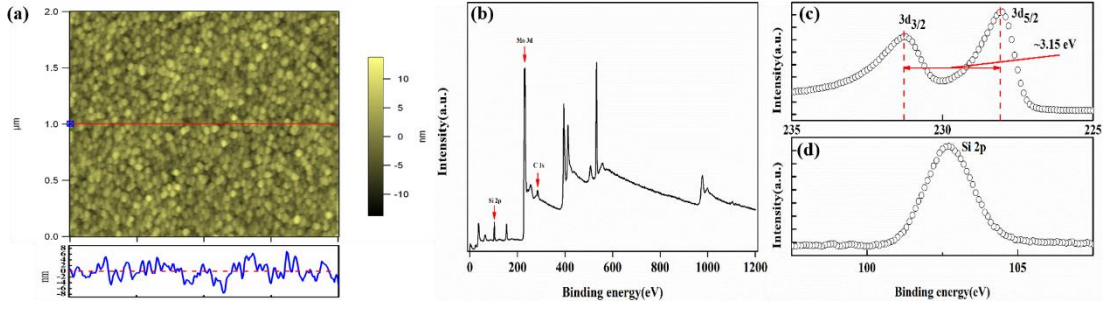


Figure 1 (a) AFM topographical image and the corresponding cross-section profile, and (b) XPS full spectrum of MoSi thin film. XPS spectra of (c) Mo 3d and (d) Si 2p were used to obtain the chemical composition of MoSi thin film.

Figure 1 (a) shows the surface morphology and the corresponding cross-section profile of MoSi thin film, demonstrating the uniform crack-free microstructure with root-mean-square surface roughness of  $4.2 \pm 0.1$  nm. Figure 1 (b) depicts the XPS full spectrum of MoSi thin film, indicating the existence of Mo and Si elements, as marked by the red arrow. Additionally, high-resolution XPS results of Mo 3d and Si 2p are given in Figure 1(c) and (d), respectively. Two peaks centered at 228.00 eV and 231.20 eV, corresponding to  $3d_{5/2}$  and  $3d_{3/2}$ , respectively, are observed in Mo 3d XPS spectrum, due to the spin-orbital coupling effect. The binding energies and the corresponding spin-orbit splitting energy ( $\sim 3.15$  eV) are consistent with the previously reported results in the case of MoO<sub>2</sub>, implying the +4 valence state of molybdenum element in MoSi thin film [23]. As shown in Figure 1(d), the Si 2p XPS spectrum exhibits a high symmetric peak, as similarly observed in other amorphous materials [24]. This behavior is usually ascribed to the widening effect, which dissolves the asymmetry characteristic originating from the spin-orbital coupling effect. Also, the -4 valence state of silicon element was confirmed in MoSi thin film [25]. Furthermore, from the XPS spectra of Si 2p and Mo 3d, the chemical composition ratio of MoSi thin film is obtained to be around  $1.00 \pm 0.04$ .

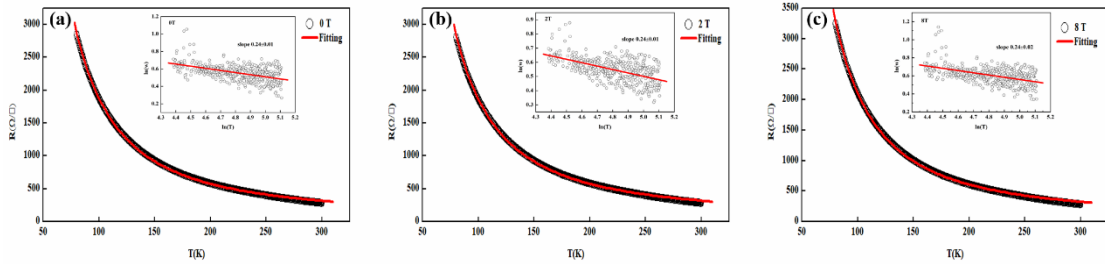


Figure 2 Temperature-dependent sheet resistance and the corresponding Zabrodskii analysis (inset) at different magnetic field, (a) 0T, (b) 2T, (c) 8T. The red solid lines in figures show the fitting results.

Figure 2 depicts the temperature-dependence of sheet resistance under different magnetic field, demonstrating the semiconductor behaviors in the measured temperature region. According to the previous reports on the electro-transport behaviors of amorphous alloys [26, 27], the thermal activation model and the variable-range hopping (VRH) model were generally utilized to analyze the conduction mechanism. Here, a self-consistent method, *i.e.*, Zabrodskii analysis [28], was used to specifically decide the mechanism. The logarithmic derivative  $w = -d(\ln(R))/d(\ln(T)) = p \cdot (T_0/T)^p$  is introduced, where

$T_0$  is the characteristic parameter,  $T$  is the temperature, and  $p$  is the exponential term [29]. Different  $p$  values correspond to different conduction mechanisms, for example, the thermal activation model ( $p=1$ ), the Mott-VRH model ( $p=1/4$ ) [30], and the Efros-Shklovskii (ES) VRH model ( $p=1/2$ ) [31]. As shown in the insets of Figure 2, obviously,  $\ln(w)$  exhibits the linear dependence on  $\ln(T)$ , and all the slopes of  $\sim 1/4$  were determined, indicating the Mott-VRH conduction mechanism in the MoSi thin film, as analogously reported in other amorphous binary compounds [21]. Additionally, from the Mott-VRH fitting, as shown in Figure 2 (red solid lines), the characteristic parameter,  $T_0$ , would be calculated to be  $3.05 \times 10^5$  K (0T),  $2.85 \times 10^5$  K (2T) and  $3.73 \times 10^5$  K (8T) for the MoSi thin film.  $T_0$  decreases first and then increases as the magnetic field increases from 0T to 8T. According to the equation  $T_0 = 18.1/(k_B g_0 a_0^3)$  ( $g_0$  is the constant Mott density of states and  $a_0$  is the localization length) [30], the trend of  $a_0$  is opposite to that of  $T_0$ . The variation of the localization length,  $a_0$ , with applied magnetic field might indicate the interesting magneto-resistance (MR) behavior, as discussed below.

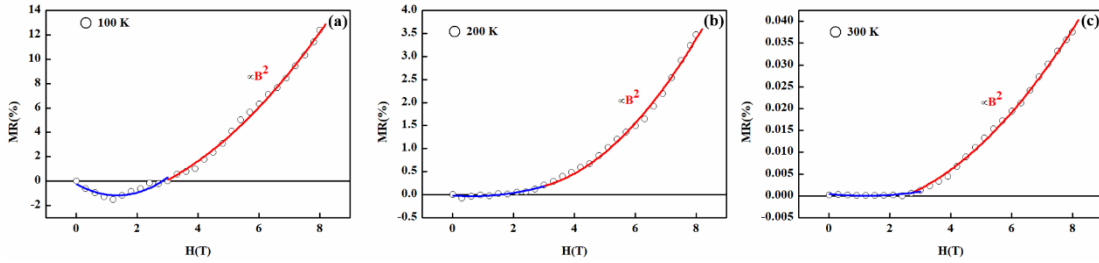


Figure 3 Magnetic-field dependence of MR in MoSi thin film at different temperatures, (a) 100 K, (b) 200 K, (c) 300 K.

Figure 3 presents the magnetic-field dependent MR at different temperatures. Here, MR is defined as  $MR=(R(H)-R(0))/R(0) \times 100\%$ , where  $R(H)$  and  $R(0)$  are the sheet resistance of MoSi thin film at magnetic field of  $H$  and zero, respectively. With increasing magnetic field, the obvious crossover from negative to positive MR could be observed at low temperature, *i.e.*, 100K. With increasing temperature, the negative MR characteristic was weakened and disappeared at high temperature, *i.e.*, 300K. Similar phenomena were observed in some amorphous materials, for example,  $Ni_xSi_{1-x}$  [21]. Generally, MR consists of positive MR (pMR) and negative MR (nMR):

$$MR=pMR+nMR$$

The pMR is closely related to the wave-function shrinkage effect [32, 33]. Under magnetic field, the electron wave-function will be shrunk, and thus the hopping probability of electrons between the two sites will be reduced, resulting in pMR. The relationship between pMR and magnetic field  $H$  can be expressed as  $pMR \propto H^2$  [34]. As expected, the fitting results (red solid lines in Figure 3) are very consistent with the experimental data. On the other hand, different from pMR, nMR is closely associated with the electron wave-function interference effect [34]. When electrons hop between two sites, the wave-function interference along random paths will occur, and in turn will change the hopping probability between two sites. It should be noted that this interference effect is pronounced at low temperature [35]. An empirical equation [21],  $nMR \propto -H$ , was generally used to describe the nMR caused by the interference effect. In our case, obviously, the negative MR is attributed to the competition of the wave function shrinkage effect and the interference effect. For example, at 100 K (as shown in Figure 3(a)), with increasing magnetic field, pMR is cancelled first by nMR, resulting in a

whole negative MR, and subsequently the contribution of nMR is reduced and thus the positive MR is observed. With increasing temperature, the interference effect is weakened, probably due to the enhanced jump probability between the two nearest neighbors, resulting in the reduced possible hopping paths of one site. Accordingly, the contribution of nMR is reduced and thus the negative MR characteristic is not obvious at high temperature (as shown in Figure 3(b) and (c)). Additionally, as mentioned above, the localization length,  $a_0$ , increases with increasing magnetic field from 0T to 2T, indicating the increased interference effect and the corresponding negative MR. With further increasing magnetic field from 2T to 8T, the localization length,  $a_0$ , decreases, indicating the increased shrinkage effect and the corresponding positive MR.

#### 4. Conclusions

In summary, the MoSi amorphous films were grown on silicon substrates at room temperature by RF magnetron sputtering technique, and the electronic transport and magneto-transport behaviors in the non-superconducting region were studied. The temperature-dependent resistance was analyzed through a self-consistent method, and the Mott-VRH transport mechanism was confirmed. The crossover from negative to positive MR was observed with increasing magnetic field. The positive MR is primarily ascribed to the electron wave-function shrinkage effect, whereas the negative MR is mainly attributed to the electron wave-function interference effect.

#### Acknowledgements

This work was supported by the National Key Research and Development Program of China (2017YFB0503300) and the Fundamental Research Funds for the Central Universities (Nos. 310201911cx024, 310201911fz048).

#### References

- [1] B. Baeka, A.E. Lita, V. Verma, S.W. Nam, *Appl. Phys. Lett.* **98** (2011) 251105.
- [2] V.B. Verma, A.E. Lita, M.R. Vissers, F. Marsili, D.P. Pappas, P.R. Mirin, S.W. Nam, *Appl. Phys. Lett.* **105** (2014) 022602.
- [3] A. Banerjee, L.J. Baker, A. Doye, M. Nord, R.M. Heath, K. Erotokritou, D. Bosworth, Z.H. Barber, I. MacLaren, R.H. Hadfield, *Supercond. Sci. Tech.* **30** (2017) 084010.
- [4] M.M. Collver, R.H. Hammond, *Phys. Rev. Lett.* **30** (1973) 92.
- [5] V.B. Verma, B. Korzh, F. Bussi ères, R.D. Horansky, S.D. Dyer, A.E. Lita, I. Vayshenker, F. Marsili, M.D. Shaw, H. Zbinden, R.P. Mirin, S.W. Nam, *Opt. Express* **23** (2015) 33792.
- [6] H.T. Huy, H. Shishido, M. Hayashi, T. Yotsuya, M. Kato, T. Ishida, *Physica C* **484** (2013) 86.
- [7] M.L. Liang, M.N. Kunchur, 2010 *Phys. Rev. B* **82** (2010) 144517.
- [8] F. Colauto, M. Motta, A. Palau, M.G. Blamire, T.H. Johansen, W.A. Ortiz, *IEEE T. Appl. Supercond.* **25** (2015) 1.
- [9] M. Motta, F. Colauto, J.I. Vestg ården, J. Fritzsche, M. Timmermans, J. Cuppens, C. Attanasio, C. Cirillo, C.C. Moshchalkov, J.V. Vondel, T.H. Johansen, W.A. Ortiz, A.V. Silhanek, *Phys. Rev. B* **89** (2014) 134508.
- [10] C.M. Natarajan, M.G. Tanner, R.H. Hadfield, *Supercond. Sci. Tech.* **25** (2012) 63001.
- [11] Y.P. Korneeva, M.Y. Mikhailov, Y.P. Pershin, N.N. Manova, A.V. Divochiy, Y.B. Vakhtomin, A.A. Korneev, K. V. Smirnov, A.G. Sivakov, A.Y. Devizenko, G.N. Goltsman, *Supercond. Sci. Tech.* **27** (2014) 95012.
- [12] M. Caloz, B. Korzh, N. Timoney, M. Weiss, S. Gariglio, R.J. Warburton, C. Sch änenberger, J. Renema, H. Zbinden, F. Bussi ères, *Appl. Phys. Lett.* **110** (2017) 083106.

- [13] H.B. Zhang, L. Xiao, B.C. Luo, J.H. Guo, L.B. Zhang, J. Xie, *J. Phys. D: Appl. Phys.* **53** (2020) 013001.
- [14] L. Ceccarelli, D. Vasyukov, M. Wyss, G. Romagnoli, N. Rossi, L. Moser, M. Poggio, *Phys. Rev. B* **100** (2019) 104504.
- [15] G. Grimaldi, A. Leo, P. Sabatino, G. Carapella, A. Nigro, S. Pace, V.V. Moshchalkov, A.V. Silhanek, *Phys. Rev. B* **92** (2015) 024513.
- [16] A. Leo, G. Grimaldi, A. Nigro, E. Bruno, F. Priolo, S. Pace, *Physica C* **503** (2014) 140.
- [17] N. Kokubo, H. Tamochi, B. Shinozaki, T. Nishizaki, N. Kobayashi, *J. Phys. Conf. Ser.* **400** (2012) 022057.
- [18] S. Okuma, D. Shimamoto, N. Kokubo, *Phys. Rev. B* **85** (2012) 064508.
- [19] S. Ikeda, K. Miura, H. Yamamoto, K. Mizunuma, H.D. Gan, M. Endo, S. Kanai, J. Hayakawa, F. Matsukura, H. Ohno, *Nat. Mater.* **9** (2010) 721.
- [20] H. Mell, J. Stuke, *J. Non-cryst. solids* **4** (1970) 304.
- [21] R. Rosenbaum, T. Murphy, E. Palm, S. Hannahs, B. Brandt, *Phys. Rev. B* **63** (2001) 094426.
- [22] S. Yoshizumi, T. H. Geballe, M. Kunchur, W.L. McLean, *Phys. Rev. B* **37** (1988) 7094.
- [23] J. G. Choi, L.T. Thompson, *Appl. Surf. Sci.* **93** (1996) 143.
- [24] F.R. Lamastra, S. Mori, V. Cherubini, M. Scarselli, F. Nanni, *Mater. Chem. Phys.* **194** (2017) 253.
- [25] S.A. Mironov, V.P. Dubkov, K.V. Chizh, V.A. Yuryev, *J. Phys. Conf. Ser.* **816** (2017) 012011
- [26] S.K. Sharma, R.K. Shukla, A. Kumar, *Physica B* **481** (2016) 144.
- [27] Deepika, H. Singh, *Can. J. Phys.* **97** (2019) 222.
- [28] A.G. Zabrodskii, *Philos. Mag. B* **81** (2001) 1131.
- [29] B.C. Luo, J.B. Hu, *ACS Appl. Electron. Mater.* **1** (2019) 51.
- [30] N.F. Mott, *J. Non-cryst. solids* **1** (1968) 1.
- [31] A.L. Efros, B.I. Shklovskii, *J. Phys. C: Solid State Phys.* **8** (1975) L49.
- [32] W. Schoepe, *Physik B - Condensed Matter* **71** (1988) 455.
- [33] B.I. Shklovskii, A.L. Efros, *Electronic Properties of Doped Semicondors*, 1<sup>st</sup> ed., Springer, Dordrecht, 1984.
- [34] V.L. Nguyen, B.Z. Spivak, B.I. Shklovskii, *J. Exp. Theoretical Phys.* **62** (1985) 1021.